

## In-situ chemical imaging of solid-electrolyte interphase layer evolution in Li-S batteries

Manjula I. Nandasiri, Luis Eduardo Camacho-Forero, Ashleigh M Schwarz, Vaithiyalingam Shutthanandan, Suntharampillai Thevuthasan, Perla B. Balbuena, Karl T. Mueller, and Vijayakumar Murugesan

*Chem. Mater.*, **Just Accepted Manuscript** • Publication Date (Web): 03 May 2017

Downloaded from <http://pubs.acs.org> on May 4, 2017

### Just Accepted

“Just Accepted” manuscripts have been peer-reviewed and accepted for publication. They are posted online prior to technical editing, formatting for publication and author proofing. The American Chemical Society provides “Just Accepted” as a free service to the research community to expedite the dissemination of scientific material as soon as possible after acceptance. “Just Accepted” manuscripts appear in full in PDF format accompanied by an HTML abstract. “Just Accepted” manuscripts have been fully peer reviewed, but should not be considered the official version of record. They are accessible to all readers and citable by the Digital Object Identifier (DOI®). “Just Accepted” is an optional service offered to authors. Therefore, the “Just Accepted” Web site may not include all articles that will be published in the journal. After a manuscript is technically edited and formatted, it will be removed from the “Just Accepted” Web site and published as an ASAP article. Note that technical editing may introduce minor changes to the manuscript text and/or graphics which could affect content, and all legal disclaimers and ethical guidelines that apply to the journal pertain. ACS cannot be held responsible for errors or consequences arising from the use of information contained in these “Just Accepted” manuscripts.

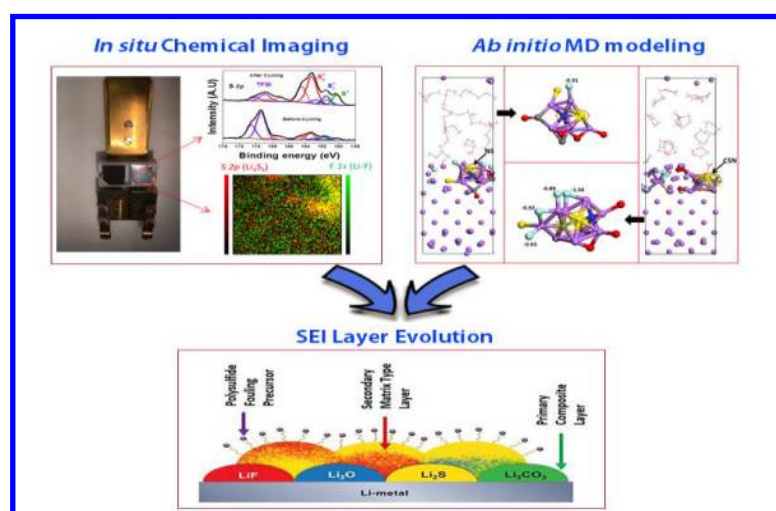
# *In-situ chemical imaging of solid-electrolyte interphase layer evolution in Li-S batteries*

Manjula I. Nandasiri<sup>a†</sup>, Luis E. Camacho-Forero<sup>b</sup>, Ashleigh M. Schwarz<sup>a</sup>, Vaithiyalingam Shutthanandan<sup>a</sup>, Suntharampillai Thevuthasan<sup>a</sup>, Perla B. Balbuena<sup>b</sup>, Karl T. Mueller<sup>a,c</sup>, and Vijayakumar Murugesan<sup>\*a,c</sup>

<sup>a</sup> Pacific Northwest National Laboratory, Richland, WA 99354, USA.

<sup>b</sup> Department of Chemical Engineering, Texas A&M University, College Station, Texas 77843, USA.

<sup>c</sup> JCESR, Pacific Northwest National Laboratory, Richland, WA 99354, USA.



**ABSTRACT:** Parasitic reactions of electrolyte and polysulfide with the Li-anode in lithium sulfur (Li-S) batteries lead to the formation of solid-electrolyte interphase (SEI) layers, which are the major reason behind severe capacity fading in these systems. Despite numerous studies, the evolution mechanism of the SEI layer and specific roles of polysulfides and other electrolyte components are still unclear. We report an in-situ X-ray photoelectron spectroscopy (XPS) and chemical imaging analysis combined with *ab initio* molecular dynamics (AIMD) computational modeling to gain fundamental understanding regarding the evolution of SEI layers on Li-anodes within Li-S batteries. A multi-modal approach involving AIMD modeling and in-situ XPS characterization uniquely reveals the chemical identity and distribution of active participants in parasitic reactions as well as the SEI layer evolution mechanism. The SEI layer evolution has three major stages: the formation of a primary composite mixture phase involving stable lithium compounds ( $\text{Li}_2\text{S}$ ,  $\text{LiF}$ ,  $\text{Li}_2\text{O}$  etc); and formation of a secondary matrix type phase due to cross interaction between reaction products and electrolyte components, which is followed by a highly dynamic mono-anionic polysulfide (i.e.  $\text{LiS}_5$ ) fouling process. These new molecular-level insights into the SEI layer evolution on Li- anodes are crucial for delineating effective strategies for the development of Li-S batteries.

## Introduction

The lithium-sulfur (Li-S) battery is a promising candidate for next generation energy storage due to its high theoretical specific capacity ( $1675 \text{ mA}\cdot\text{h}\cdot\text{g}^{-1}$ ) and up to five-fold increase in energy density ( $2567 \text{ W}\cdot\text{h}\cdot\text{Kg}^{-1}$ ) as compared to state-of-the-art lithium-ion batteries (LIBs).<sup>1-5</sup> However, there are critical challenges to overcome to realize the commercialization of Li-S batteries (LSBs). One of the most demanding challenges is effectively protecting the Li-metal anode from parasitic reactions that cause insulating solid-electrolyte interphase (SEI) layer formation, which seriously limits the capacity retention and life cycles.<sup>6-9</sup> Parasitic chemistry at the Li-metal anode is typically a combination of redox, decomposition, substitution and coordination reactions depending on the choice of electrochemistry and electrolyte materials. For example, in the Li-S electrochemical system, the elemental sulfur cathode ( $\text{S}_8$ ) is reduced to  $\text{Li}_2\text{S}$  through multiple intermediate lithium polysulfide species ( $\text{Li}_2\text{S}_x$ ;  $x \leq 8$ ) during the discharge process.<sup>3</sup> The longer chain lithium polysulfide species ( $\text{Li}_2\text{S}_x$ ;  $x \geq 6$ ) are highly soluble in electrolyte solvents and can diffuse to the Li-anode, causing complex redox and/or complexation reactions. Although molecular level details of polysulfide reactions with Li-metal are still unknown, it is hypothesized that polysulfides reduce to insoluble  $\text{Li}_2\text{S}$  and  $\text{Li}_2\text{S}_2$  species with subsequent SEI layer formation.<sup>10-11</sup> In addition to the polysulfides, highly reactive transient species arising from decomposition of electrolyte components (such as solvents and counter anions) can also be part of parasitic chemical reactions leading to subsequent SEI layer evolution.<sup>12-13</sup> This parasitic chemistry involving many complex reactions and transient molecules creates the chemically and topographically inhomogeneous SEI layer on the active Li-anode surfaces. Such a sporadic fouling process can increase the interfacial resistance for  $\text{Li}^+$  ion diffusion due to the thick deposits of insulating and insoluble species on Li-anodes.<sup>2</sup> In order to limit the complex parasitic reaction at Li-anodes and improve the performance of LSBs, it is important to unravel the mechanisms of parasitic chemistry and subsequent SEI layer formation. In particular, gaining a real time perspective of the SEI layer evolution is both critical and extremely challenging, as many of its constituents and originating reactions are transient and highly air-sensitive in nature.<sup>14</sup> Few experimental techniques are capable of probing the SEI layer formation and *ab initio* based computational modeling were recognized as efficient and convenient tool for analysing the SEI layer formation<sup>15-18</sup>.

Despite the technical challenges in building in-situ spectroscopic and microscopic capabilities for the analysis of Li-S batteries, some efforts were made in recent years to capture the evolution and dynamic changes in the SEI layer during battery cycling.<sup>14, 19-21</sup> Nevertheless, none of the spectroscopic studies could capture the entire reaction suite and identify all constituents associated with SEI layer formation in LSBs. For example, element specific spectroscopic techniques such as nuclear magnetic resonance (NMR), electron paramagnetic resonance (EPR), and X-ray absorption spectroscopy (XAS) were able to provide only a fractional view of complex parasitic reactions by monitoring a single reactant and/or products.<sup>20, 22-28</sup> Similarly, the in-situ microscopic techniques such as transmission X-ray microscopy (TXM)<sup>29-30</sup> and X-ray fluorescence microscopy<sup>31</sup> were employed to understand the spatial evolution of SEI layers but lack the critical chemical speciation. Despite various in-situ efforts, the gap in knowledge that would provide a comprehensive understanding of SEI layer evolution at the Li-metal anode in LSBs remains and inhibits the design and formulation of optimal electrolytes<sup>32</sup>. To gain a comprehensive and molecular-level view of the parasitic reactions and subsequent SEI layer evolution, we have developed a first-of-its-kind in-situ X-ray photoelectron spectroscopy (XPS) capability that can simultaneously provide spatially resolved chemical imaging as well as chemical speciation through high resolution core-level spectroscopy of critical elements. By combining in-situ XPS results with *ab initio* molecular dynamics (AIMD) computational modeling, molecular level insight is realized regarding the distinct roles of transient species from parasitic reactions and the subsequent SEI layer evolution during cycling processes of Li-S batteries.

## Experimental details

The high vapor pressures of elemental sulfur ( $\text{S}_8$ ) and aprotic electrolyte solvents such as 1,3-dioxolane (DOL) and dimethoxyethane (DME) are the central challenge in developing in-situ XPS for Li-S batteries. To overcome this issue, we employed an ultrahigh vacuum (UHV) compatible ionic liquid (IL), 1-butyl-1-methylpyrrolidinium bis(trifluoromethylsulfonyl)imide *i.e.* [bmpyr]<sup>+</sup>[TFSI]<sup>-</sup> as a co-solvent in the electrolyte. The [bmpyr]<sup>+</sup> [TFSI]<sup>-</sup> ionic liquid used in this study has been reported as compatible electrolyte for Li-S cells due to their high electrochemical stability.<sup>33-35</sup> Various ionic liquids have also been used as electrolytes and are electrochemically stable in the voltage range ( $\pm 2.2\text{V}$ ) of Li-S batteries.<sup>36-37</sup> A solution of 1M  $\text{Li}_2\text{S}_6$  dissolved in a DOL and DME solvent mixture is prepared as reported earlier<sup>38</sup> (see SI). Subsequently, 20 wt% of the  $\text{Li}_2\text{S}_6$  in DOL and

ME solution is mixed with [bmpyr]<sup>+</sup> [TFSI]<sup>-</sup> and used as the final electrolyte system for the *in-situ* study (see SI). Apart from the vacuum compatibility, the specific choice of [TFSI]<sup>-</sup> counter anion containing IL is to ensure the electrolyte system represents the traditional Li-TFSI salt widely used in the Li-S battery studies. In addition, this electrolyte solution resembles the typical Li-S battery after the discharge cycle, where the lithium polysulfide (Li<sub>2</sub>S<sub>x</sub>) species are expected to get dissolved in DOL/DME solvent. In this case, however, the volatile sulfur cathode is replaced with graphite foil and Li<sub>2</sub>S<sub>6</sub> dissolved in the electrolyte solvent mixture is used as a sulfur source by initiating the redox process via the charging cycle. A schematic of the *in-situ* XPS sample holder is shown in Figure 1. The Li-anode and graphite-cathode materials can be mounted on a Teflon base and subsequently connected with gold wires as an external electrical contact line to the electrochemical analyzer. The reservoir in between the anode and cathode is filled with electrolyte mixture such that it covers half of the electrode surfaces. The cell is fully charged and discharged at 2.2V for two consecutive cycles only due to the limited availability of active sulfur material. All measurements are performed on the Li-electrolyte interfacial region at the end of each charge/discharge cycle to avoid the charge-induced XPS peak shifts (see SI). The graphite cathode is fully covered by ionic liquid due to high surface wetting processes (see SI).

XPS analysis was performed using a Kratos Axis Ultra DLD spectrometer, which consists of a high performance Al K $\alpha$  monochromatic X-ray source (1486.6 eV) and a high resolution hemispherical mirror analyzer. The X-ray source was operated at 150 W and emitted photoelectrons were collected at the analyzer entrance slit normal to sample surface. The data acquisition was carried out in a hybrid mode with an analysis area of 700  $\times$  300  $\mu$ m. The survey spectra were recorded at a pass energy of 160 eV with 0.5 eV step size and high resolution spectra were recorded at a pass energy of 20 eV with step size of 0.1 eV. The pass energy of 20 eV in the 700  $\times$  300  $\mu$ m analysis area is referenced to the FWHM of 0.59 eV for Ag 3d<sub>5/2</sub>. A charge neutralizer with low energy electrons was used to exclude surface charging effects and the binding energy of C 1s at 284.8 eV was used as the charge reference. The elemental and chemical state maps were acquired using the imaging XPS capability in the Kratos Axis Ultra system. The maps were collected in a field of view of 800  $\mu$ m with a spatial resolution of  $\sim$  5  $\mu$ m. The imaging XPS data were collected under a pass energy of 160 eV at each peak and background

energy. The chamber pressure was maintained at  $\leq 5 \times 10^{-9}$  Torr during all measurements. XPS data were analyzed using the CasaXPS software assuming Gaussian/Lorentzian (30% Lorentzian) line shapes and utilizing Shirley background correction. All the XPS binding energies reported here have an uncertainty of  $\pm 0.1$  eV. The background subtraction and imaging data processing were accomplished using the CasaXPS software to obtain the elemental and chemical state XPS maps presented here.

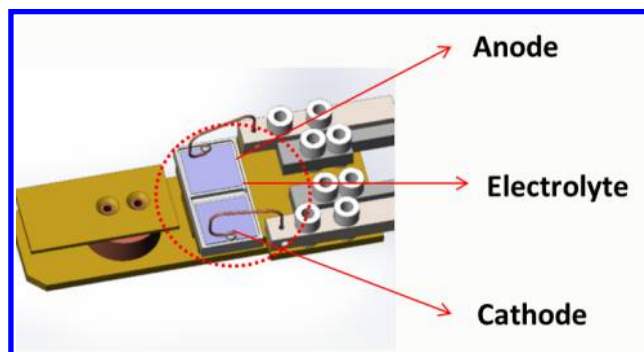


Figure 1. Schematic diagram of the XPS sample holder developed for battery cycling and *in-situ* XPS characterization.

Reaction energies for possible decomposition reactions of Li<sub>2</sub>S<sub>6</sub> at the Li-anode were calculated using Density Functional Theory (DFT) as implemented in the Gaussian 09 package<sup>39</sup> with a hybrid functional B3PW91 and the 6-311+G(3df,p) basis set. The polarizable continuum model (PCM)<sup>40</sup> was used for describing the DME solvation effects. After polysulfide and salt decompositions take place, several SEI products are formed. The analyses of these complexes (typically of the form: *X-Li-species-Li-X*) were performed on the basis of the resulting products after 20 ps of AIMD simulation of electrolyte mixtures consisting of 1 M LiTFSI in DME:DOL in contact with a Li metal surface as described in our previous study.<sup>41</sup> The Li-metal anode was modelled as a (100) Li crystallographic plane. In addition to the salt and solvent, the electrolyte also contained a 1 M Li<sub>2</sub>S<sub>8</sub> polysulfide species. Although the polysulfide used in these simulations is a longer chain than that used in the experiments, it is expected to yield almost the same final SEI components by the end of the decomposition process. The AIMD simulations were performed using the Vienna *ab Initio* Simulation Package (VASP).<sup>42-43</sup> All the AIMD calculations were based on DFT within the Perdew-Burke-Ernzerhof generalized gradient approximation (GGA-PBE).<sup>44</sup> Although the electron transfer rates may be significantly underestimated using semi-local generalized gradient approximation functionals, the AIMD results provide good insights into the

decomposition pathways and identification of products. The projector augmented wave (PAW) pseudopotentials<sup>45-46</sup> were used. The energy cut-off of the plane-wave basis expansion was set to 400 eV. A *NVT* ensemble at 330 K was used with a time step of 1 *fs* and a Nose thermostat (see our previous study<sup>41</sup> for more details). Finally, the electronic charges were calculated by using the Bader charge analysis.<sup>47-49</sup>

## Results and discussion

In-situ XPS and imaging XPS were carried out at the interfacial region between Li metal anode and IL/Li<sub>2</sub>S<sub>6</sub> electrolyte before and after charge/discharge process (see SI). The high resolution S 2*p* core level XPS spectra of Li metal anode before cycling and after each charge/discharge cycle are shown in Figure 2. The S 2*p* spectra is a doublet comprised of closely spaced spin-orbit components ( $\Delta=1.16\text{eV}$ , intensity ratio=0.511) arising from 2*p*<sub>3/2</sub> and 2*p*<sub>1/2</sub>. Each sulfur compound shows the characteristic doublet, and only the high intensity 2*p*<sub>3/2</sub> will be discussed hereafter for simplicity (see SI). The sulfone group (R-SO<sub>2</sub>-R) of the TFSI anion is observed at 169 eV along with broad sulfide peaks encompassing the 160-165 eV binding energy regime.<sup>50-51</sup> In addition, a low intensity peak at 167.2 eV representing sulfite (SO<sub>3</sub><sup>2-</sup>) or thiosulfate (S<sub>2</sub>O<sub>3</sub><sup>2-</sup>) species is also observed.<sup>52-53</sup> Deconvolution of S 2*p* spectra under the broad sulfide region gave three unique components, namely sulfide dianion (S<sup>2-</sup>) of Li<sub>2</sub>S at 160.2 eV along with terminal sulfur (S<sub>T</sub><sup>1-</sup>) and bridging sulfur (S<sub>B</sub><sup>0</sup>) of lithium polysulfide (Li<sub>2</sub>S<sub>*x*</sub> with *x*>1) at 161.6 and 163.3 eV, respectively.<sup>52, 54</sup> Based on the evolution of different sulfide concentrations (Fig.2b and Table S1) during the cycling process, we can analyze the polysulfide shuttling process and subsequent parasitic reaction with the Li-anode, which is widely believed to be a major cause for capacity loss in Li-S batteries. Similarly, the S 2*p* peak ratio between the bridging and terminal sulfur *i.e.* S<sub>B</sub><sup>0</sup>/S<sub>T</sub><sup>1-</sup> of the polysulfide species can be used as a qualitative indicator of polysulfide speciation (see SI).

Before cycling, the polysulfide components (S<sub>T</sub><sup>1-</sup> and S<sub>B</sub><sup>0</sup>) are about 22 *at.%* of total sulfur and the S<sub>B</sub><sup>0</sup>/S<sub>T</sub><sup>1-</sup> ratio is about 2.2 in accordance with our starting electrolyte mixture, which is predominantly Li<sub>2</sub>S<sub>6</sub> (Fig. 2d). After the first charge cycle, the total amount of polysulfide components increased to ~30 *at.%* whereas the lithium sulfide (S<sup>2-</sup>) concentration remains unchanged (5 *at.%* of total sulfur). During the charging process, Li<sup>+</sup> cations move towards the Li-anode and engage in the Li-plating process ( $\text{Li}^+ + e^- \rightarrow \text{Li}^0$ ). Such an electrochemically driven process

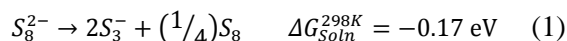
includes the Li<sup>+</sup> cations, which are part of lithium polysulfide species, and initiates the polysulfide shuttling process. Significant increase in polysulfide components after the charging cycle clearly indicates that the polysulfide shuttling process mainly depends on the Li-S interaction strength relative to Li-solvent and Li-TFSI interactions. Such a Li<sup>+</sup> driven shuttling process will lead to accumulation of polysulfide species and starts the fouling process at the Li-anode, which is followed through increased concentrations of polysulfide components in the XPS spectra after a charge cycle. Interestingly, the S<sub>B</sub><sup>0</sup>/S<sub>T</sub><sup>1-</sup> ratio increases to ~3 indicating that the parent Li<sub>2</sub>S<sub>6</sub> polysulfide species evolves into other types of polysulfide species during the fouling process, which will be discussed later.

During the discharge process the Li-anode undergoes Li-stripping processes releasing Li<sup>+</sup> and electrons, which can reduce the accumulated long chain polysulfides to lithium sulfide (S<sup>2-</sup>). Evidently the lithium sulfide (S<sup>2-</sup>) concentration is nearly doubled (~10 *at.%*) after the first discharge cycle and further increases to 15 *at.%* of the total sulfur concentration during the second charge and discharge cycles. The significant increase in S<sup>2-</sup> concentration during the discharge cycles indicates that the longer chain polysulfides accumulated at the Li-anode are being reduced to insoluble Li<sub>2</sub>S and subsequently become irreversible parts of the SEI layer during the first discharge cycle.<sup>55</sup> This Li<sub>2</sub>S formation covers the Li-anode surface and restricts further sulfide reduction during subsequent cycling processes as noted by the similar S<sup>2-</sup> concentrations in the 2<sup>nd</sup> charge and discharge cycles. Interestingly, the total amount of polysulfide components (S<sub>T</sub><sup>1-</sup> and S<sub>B</sub><sup>0</sup>) increases further to ~50 *at.%* and eventually reaches a plateau value of ~63 *at.%* during the 2<sup>nd</sup> charge/discharge cycles (see Fig. 2b). It is expected that the polysulfide will shuttle back towards the cathode side during the discharge process based on the Li<sup>+</sup> flow direction. However, we observed continuous increases in polysulfide and Li<sub>2</sub>S concentration at the Li-anode leading to loss of active materials (*i.e.*, scarcity of polysulfide solute in IL electrolyte) and subsequently causing cell failure and preventing further cycling studies. This finding indicates that the fouling process is mostly irreversible and the polysulfide is chemically interacting with the other components of the SEI layer. We postulate that various components of SEI layers can strongly interact with polysulfide solutes in the electrolyte and cause continuous fouling processes that are supported by the increase in polysulfide concentration during the cycling process (see Fig. 2b). This observation is in agreement with a previous AIMD analysis, which

predicted the clustering of polysulfide chains near the  $\text{Li}_2\text{S}$  layer as part of SEI formation.<sup>11</sup> Nevertheless, the cluster formation is favored for lower order polysulfide chains ( $\text{Li}_2\text{S}_x$  with  $x < 6$ ), which would require lower  $\text{S}_\text{B}^0/\text{S}_\text{T}^{1-}$  ratios ( $\leq 2$ ).<sup>38</sup> In addition, recent reports suggest the formation of insoluble  $\text{Li}_2\text{S}_2$  from polysulfide reduction processes at the Li-anode.<sup>56</sup> The observed increase in terminal polysulfide ( $\text{S}_\text{T}^{1-}$ ) peak intensity with cycling initially seems to support the presence of  $\text{Li}_2\text{S}_2$  species within the SEI layer (see Fig. 2b). However, any such  $\text{Li}_2\text{S}_2$  formation should significantly decrease the  $\text{S}_\text{B}^0/\text{S}_\text{T}^{1-}$  and  $\text{S}^{2-}/\text{S}_\text{T}^{1-}$  ratios. Conversely, we observed that these ratios increase with charge/discharge cycles (see Fig. 2c), which strongly suggests that  $\text{Li}_2\text{S}_2$  is not the dominant sulfide phase in the SEI layer.

Interestingly, the  $\text{S}_\text{B}^0/\text{S}_\text{T}^{1-}$  ratio of  $\sim 4$  is even higher than the possible longer polysulfide chain (*i.e.*  $\text{Li}_2\text{S}_8$  for which  $\text{S}_\text{B}^0/\text{S}_\text{T}^{1-}$  ratio is 3). Therefore, an increase in  $\text{S}_\text{B}^0/\text{S}_\text{T}^{1-}$  ratio could result from two possible scenarios: *a)* the relative concentration of terminal sulfur within the polysulfide decreases possibly due to parasitic redox reactions; or *b)* the presence of a new form of sulfur species which has the same binding energy ( $\sim 163.5$  eV) and overlaps with the  $\text{S}_\text{B}^0$  peak. Our previous studies of sulfur cathode

materials has revealed that both pristine elemental sulfur ( $\text{S}_8$ ) and carbon bonded sulfur (with  $\text{C-S}^0$  bonds) can also register  $\text{S } 2p$  peaks at the same binding energy ( $\sim 163.5$  eV) as of the bridging sulfur ( $\text{S}_\text{B}^0$ ) of the polysulfides.<sup>57</sup> Theoretical studies have predicted the formation of elemental sulfur ( $\text{S}_8$ ) as a product of dissociation of polysulfide anions (see in Li-S batteries,<sup>55</sup> via the reaction



Nevertheless, our recent AIMD simulations predicted that longer polysulfide chains are reduced very rapidly near to the Li anode.<sup>11, 41</sup> Thus, it is very unlikely to detect formation of neutral  $\text{S}_8$  on the bare surface of the Li-metal electrode. Hence, we carried out new DFT simulations to provide more insight into the possible decomposition of the precursor  $\text{Li}_2\text{S}_6$ . The calculated Gibbs free energy in DME solvent reveals two possible reduction processes,

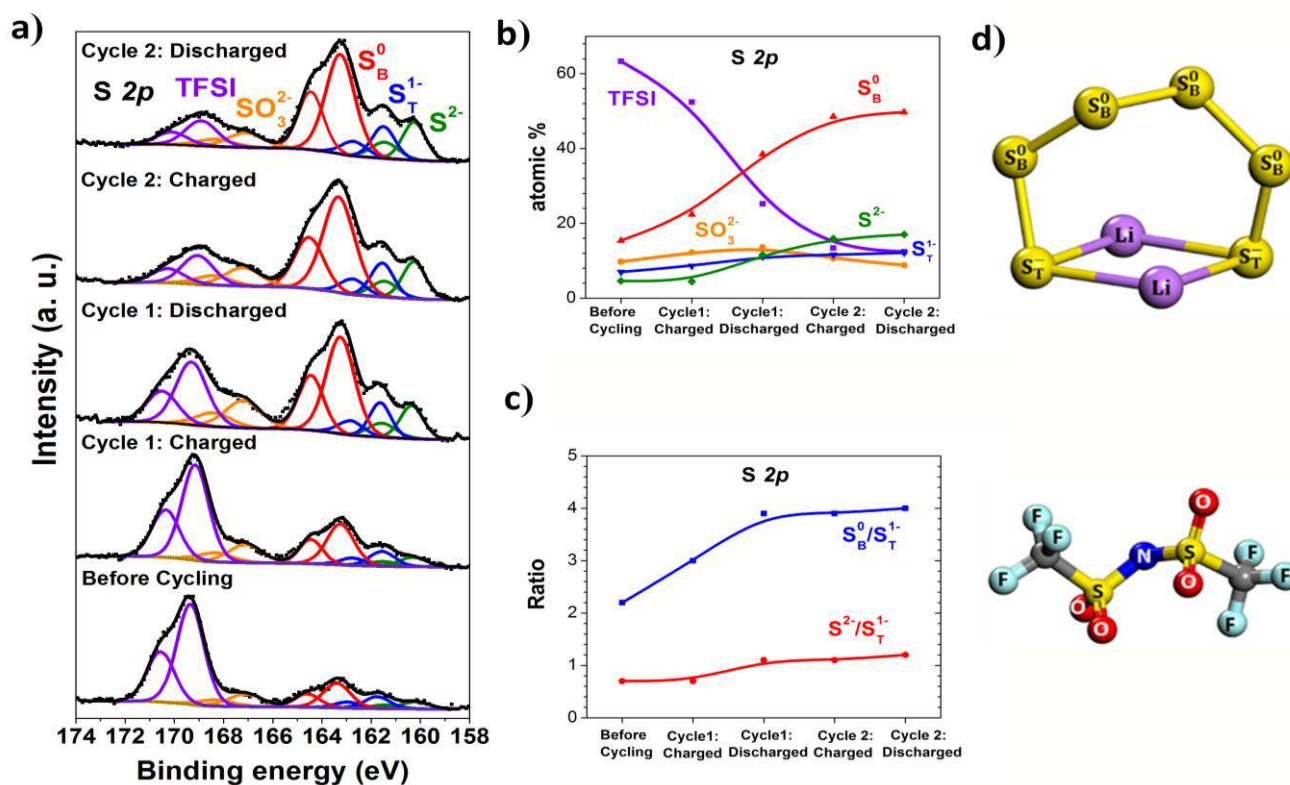
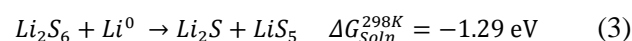
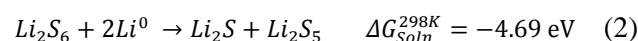


**Figure 2.** (a) Core level  $\text{S } 2p$  XPS spectra of the Li-electrolyte interfacial region with charge/discharge cycles (b) Evolution of various sulfur based species over charge/discharge cycles based on atomic concentration derived from  $\text{S } 2p$  peak areas (c) The ratio between terminal sulfide and bridging sulfur atoms ( $\text{S}_\text{B}^0/\text{S}_\text{T}^{1-}$ ) along with the disulfide and sulfide ratio ( $\text{S}^{2-}/\text{S}_\text{T}^{1-}$ ) derived from  $\text{S } 2p$  peak areas (d) Molecular structure of lithium polysulfide  $\text{Li}_2\text{S}_6$  (top) and TFSI anion (bottom) with chemical labels used in the XPS analysis.

Our DFT results indicate that the reduction product of  $\text{Li}_2\text{S}_5$  is energetically favorable (Eq.2) but represents a  $\text{S}_\text{B}^0/\text{S}_\text{T}^{1-}$  ratio of 1.5. Despite its favourable formation energy ( $\Delta G_{\text{soln}}$ ), the  $\text{Li}_2\text{S}_5$  formation requires a higher concentration of  $\text{Li}^0$  (*i.e.*, prevalent access to Li-metal surface) relative to the  $\text{LiS}_5$  formation process. This implies that, with restricted access to Li-metal, the reduction product of  $\text{LiS}_5$  would be more probable (see Eq.2 & 3). Formation of  $\text{LiS}_5$  ( $\text{S}_\text{B}^0/\text{S}_\text{T}^{1-} = 4$ ) can account for the simultaneous increase of both  $\text{Li}_2\text{S}$  concentration and  $\text{S}_\text{B}^0/\text{S}_\text{T}^{1-}$  ratio ( $\sim 3.9$ ) observed in the in-situ XPS results (see Fig. 2c). Such a reduction process can occur at the terminal sulfur atom of polysulfide molecule (*i.e.*  $\text{S}_\text{T}^{1-}$  to  $\text{S}^2$ ), which will result in a significant increase in the  $\text{S}_\text{B}^0/\text{S}_\text{T}^{1-}$  ratio and  $\text{S}^{2-}$  concentration, agreeing with our observations (see Fig. 2c). However, the long term stability of  $\text{LiS}_5$  molecule within the SEI layer still needs to be evaluated further with other analytical techniques.

In addition to the polysulfide shuttling, the SEI layer formation would also depend on the TFSI anion

decomposition process. The decomposition of TFSI anion can be simultaneously monitored by the evolution of sulfone and sulfite peaks observed in the higher binding energy regime ( $>166$  eV) in the S 2p spectra (see Fig. 2a). Before cycling, the sulfone peak from TFSI species represents  $\sim 63$  at.% of total sulfur concentration on the Li-anode. During the 1<sup>st</sup> charge and discharge cycles, the amount of sulfone species drops to  $\sim 53$  and 27 at.%, respectively. Subsequently, after the 2<sup>nd</sup> charge and discharge cycles, it drops to about 20 at.%, relative to sulfide and polysulfide concentrations (see Fig. 2c). Such a significant drop in the pristine TFSI anion concentration on the Li-anode indicates two possible mechanisms: a) a set of redox reactions altering the sulfone group as part of TFSI decomposition, b) displacement of some TFSI molecules by polysulfide species at the Li-anode surface due to the SEI layer formation process within the XPS analysis volume. Recently Y. Cui *et al* suggested that the sulfone group of TFSI anion can undergo oxidation processes at the Li-anode and produce sulfite ( $\text{SO}_3^{2-}$ ) and

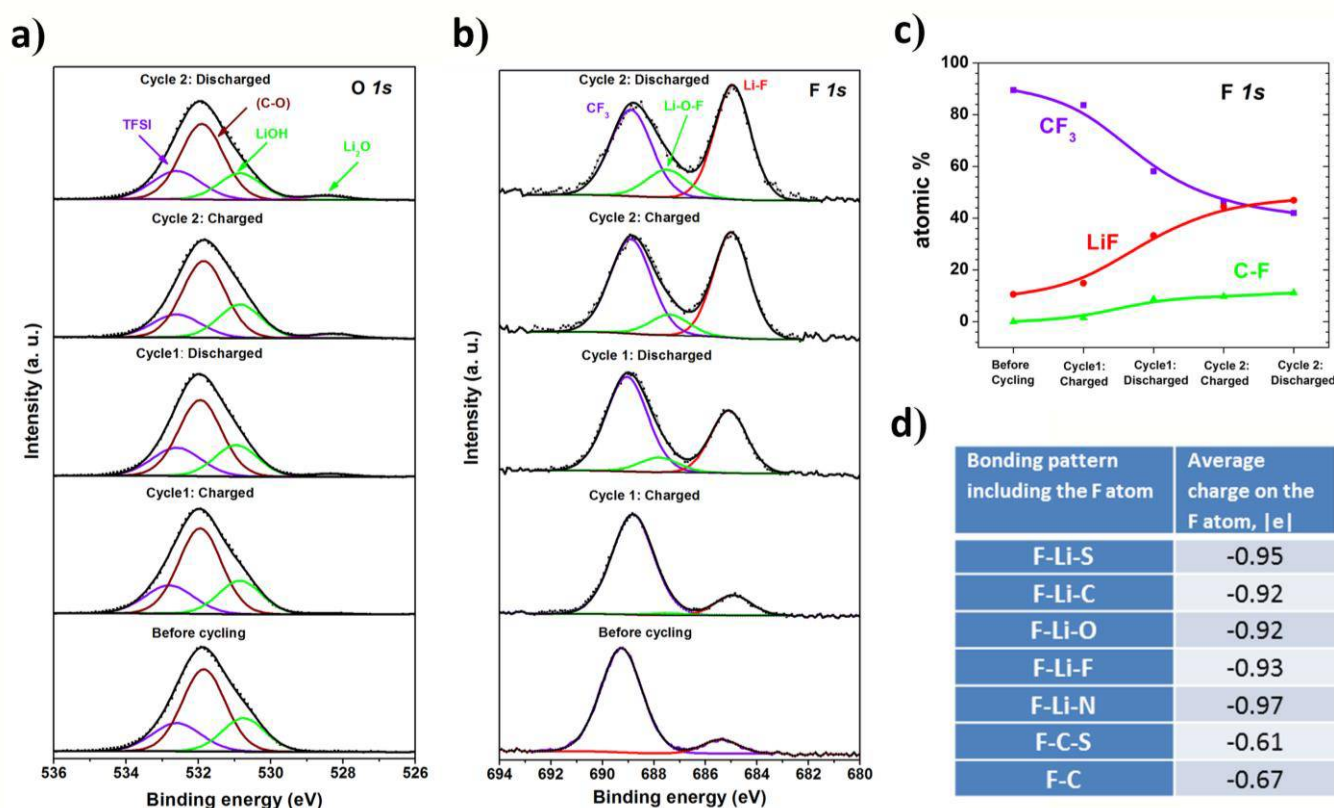


**Figure 3.** (a) Core level O 1s XPS spectra of the Li-electrolyte interfacial region with charge/discharge cycles (b) Core level F 1s XPS spectra of Li-electrolyte interfacial region with charge/discharge cycles (c) Evolution of various fluorine based species over charge/discharge cycles based on atomic concentration derived from respective F 1s peak areas (d) The various fluoride based species from TFSI decomposition predicted from AIMD calculations along with their respective electronic charges.

sulfate ( $\text{SO}_4^{2-}$ ) species based on XPS analysis.<sup>56</sup> However, they did not consider the sulfur spin-orbit based doublet in their peak deconvolution and the reported ( $\text{SO}_4^{2-}$ ) species peak ( $\sim 170$  eV) falls within the S  $2p_{1/2}$  component of the sulfone group of a pristine TFSI molecule. Our results do not show the presence of any sulfate but only the sulfite ( $\text{SO}_3^{2-}$ ) species, which shows minimal changes during the cycling process ( $\sim 4$  at.%) and fails to account for the significant drop in pristine TFSI concentration (see Fig. 2c). Decomposition of the sulfone group and formation of  $\text{Li}_2\text{S}_2\text{O}_4$  and  $\text{Li}_2\text{SO}_3$  were proposed in the literature, and this mechanism can explain the low intensity sulfite peak ( $\sim 10$  at.%) observed at  $\sim 167$  eV during the cycling process.<sup>58-59</sup> The other possibility would be the reduction of the sulfone group of the TFSI molecule to sulfur ( $\text{S}^0$ ), which will fall in the sulfide regime of the XPS spectra and thereby increase the  $\text{S}_B^0/\text{S}_T^{1-}$  ratio. However, unless the sulfone group of a TFSI anion undergoes multi-electron reduction (from  $\text{S}^{+6}$  to  $\text{S}^0$ ) at the Li-metal anode, the decomposed products are expected to be at higher binding energy ( $>166$  eV) similar to the sulfite/thiosulfate or sulfone regions. Since multi-electron reduction is less likely, we do not expect significant increase in  $\text{S}^0$  due to this mechanism. The second scenario would be displacement of TFSI anions by the polysulfide fouling process discussed earlier. Typically, the TFSI anion can interact with the counter ion from the IL (i.e.  $[\text{bmpyr}]^+$ ), Li-anode, and  $\text{Li}^+$  from the polysulfide species. During the cycling process, we observed that the polysulfide reduces to insoluble  $\text{Li}_2\text{S}$ , which can grow as a passivating film on the Li-anode surface.<sup>11, 41</sup> Such a  $\text{Li}_2\text{S}$  passivation layer can inhibit the  $\text{Li}^+$ -TFSI interactions and enhance the  $[\text{bmpyr}]^+$ -TFSI ion pairing. However, it should be noted that the  $\text{Li}_2\text{S}$  passivation layer is unlikely to be uniform and the TFSI anion will compete for interactions with the exposed Li-anode surfaces (*vide infra*) and cause the TFSI decomposition process. The TFSI anion decomposition is a cascade process with many transient species including sulfone and fluoride groups, which can subsequently interact with lithium polysulfide molecules and the Li-anode.<sup>41</sup> This process supports our previous discussion regarding the polysulfide species interacting with other components of the SEI layer and causing continuous fouling processes on the Li-anode. This clustering process will be further justified a posteriori below using other elemental analysis.

The TFSI anion decomposition process at the Li-anode can be followed through O  $1s$  and F  $1s$  spectra for deeper understanding of the SEI layer formation.

The O  $1s$  spectra is dominated by a broad peak centered around 532 eV, which can be assigned to C-O bonds within DOL/DME (electrolyte solvents) as well as lithium carbonate (Li-metal surface impurity) owing to their small chemical shift differences (see Fig. 3a).<sup>58, 60</sup> Deconvolution of the broad O  $1s$  spectra revealed shoulder peaks at  $\sim 532.6$  eV and 530.6 eV indicating the S-O bonds (sulfone and sulfite) and lithium hydroxide (Li-metal surface impurity), respectively.<sup>60</sup> There is no significant change in the concentration of these oxygen species during the cycling process. We also observe a low intensity ( $\sim 3$  at.%) peak at 528.5 eV with the cycling process indicating lithium oxide ( $\text{Li}_2\text{O}$ ) formation at the Li-anode as a result of TFSI decomposition. Although, the decomposition of the sulfone group can cause  $\text{Li}_2\text{O}$  formation,<sup>41</sup> the presence of carbonate and hydroxide native impurities at the Li-anode surface (see Fig. S4) can also lead to lithium oxide. The main product of TFSI decomposition would be lithium fluoride (LiF) formation from C-F bond breaking at the Li-anode.<sup>41</sup> Such a decomposition process can be analyzed through F  $1s$  spectra (see Fig. 3b). The F  $1s$  spectra show a dominant TFSI anion peak ( $\text{CF}_3$ ) at 688.8 eV along with a low intensity Li-F related species peak around 685 eV.<sup>50, 58, 60</sup> The Li-F related species formation even before the cycling process demonstrates the instability of TFSI anions on the Li-metal anode. The concentration of Li-F species is about 11 at.% of total fluorine before cycling and increases to 15 at.% following the 1<sup>st</sup> charging cycle (see Table S2). During the subsequent discharge cycle, the amount of this Li-F based species more than doubles to ( $\sim 33$  at.% (see Figure 3c). Such a substantial increase in the amount of Li-F species must correlate to accelerated decomposition of the TFSI anion during the discharge process. This peak at  $\sim 685$  eV in the F  $1s$  spectra is widely reported as evidence of LiF formation.<sup>61-64</sup> In addition, a new shoulder peak ( $\sim 687.5$  eV) arises near the parent  $\text{CF}_3$  peak following the charge/discharge process, which is traditionally assigned to C-F intermediate species as part of TFSI decomposition.<sup>41, 65</sup> However, such a simplified peak assignment can hinder deeper understanding of the SEI layer evolution. To clearly identify the possible fluoride species within the SEI layer, we analyzed various components of TFSI decomposition products predicted by our previous AIMD simulations<sup>41</sup> (see Fig S5-S7). Since the charge state of an atomic site dictates the binding energy of XPS spectra, we analyzed the average electronic charges of the F atom for various decomposition products and relevant fluoride atomic arrangements along with their average charge as shown in Figure 3d. These fluorine containing species generally fall in two categories based on the





mechanism of SEI layer formation is still elusive, mainly due to extreme complexity involving parasitic reaction rate, Li-anode surface chemistry and the concentration gradient of solutes. In particular, the concentration gradient of solutes at the interfacial regime can dictate the composition of the cluster and subsequent SEI layer nucleation and growth phenomena.<sup>67</sup>

We also employed XPS spectromicroscopy to analyze the underlying growth mechanism of the SEI layer, which can provide realistic views of concentration gradients in the spatial domain.<sup>68-69</sup> Figure 4 shows a two dimensional chemical imaging performed at the same spot on the Li-anode after the first charge/discharge process (see SI). The interfacial region (800 X 800  $\mu\text{m}$ ) is scanned at 685 eV (*F1s*; Li-F species) and 163.3 eV (*S 2p*;  $\text{S}_\text{B}^0$ ) binding energies to monitor the TFSI anion and polysulfide gradient with a spatial resolution of about 5  $\mu\text{m}$ . The contour mapping of chemical imaging clearly shows the clustering of reactive solutes - polysulfide (blue) and Li-F related species (red) - within the top layers of anode - electrolyte interfacial region, which can subsequently precipitate as an SEI layer (Fig. 4a & 4b). Since the XPS imaging is typically dominated by the concentration gradient of the top layer (< 5 nm) within the interfacial regime, the delimited white background represents SEI layers adjacent to the Li-anode surface with relatively lower concentration of polysulfide and LiF. It should be noted that the discharge cycle has a higher concentration of polysulfide and Li-F species than the during the charge cycle. The rise in polysulfide concentration after the discharge cycle simply reflects the expected polysulfide shuttling towards the Li-anode. Such clustering of polysulfide at the interfacial region can facilitate  $\text{Li}_2\text{S}$  precipitation as a SEI layer due to possible reduction reactions (see Eq.2 & 3). Similarly, the clustering of Li-F species can cause precipitation of lithium fluoride (LiF) phases within the SEI layer. The presence of well separated clusters of polysulfide (blue) and Li-F (red) represents the nucleation seeds for  $\text{Li}_2\text{S}$  and LiF phases and evolve as a dominant part of SEI layer evolution. Intriguingly, the total Li-F species raises along with polysulfide from the shuttling process during the discharge cycle, indicating that the  $\text{F}^-$  anion from TFSI decomposition interacts with lithium polysulfide (see Fig .4b). The overlapped signal (black) in the imaging map indicates a possible cross-interaction between  $\text{F}^-$  anion and lithium polysulfides. This corroborates our *a priori* assumption that the reactive transient species involving polysulfide and fluoride anion can chemically interact and initiate clustering with

various electrolyte components. For example, AIMD computational results predicted multiple types of Li-F species involving various electrolyte components (see Fig. 4c and Supporting Information), which could also be part of clustering phenomena that can initiate the precipitation as part of SEI layer.

Combining high resolution XPS and chemical imaging analysis with AIMD computational modeling results, we can begin unravelling the SEI layer growth mechanism. The SEI layer is commonly viewed as a multiphase material with chemically distinctive phases (such as LiF,  $\text{Li}_2\text{S}$ ,  $\text{Li}_2\text{O}$  and  $\text{Li}_2\text{CO}_3$ ) separated by well-defined boundaries<sup>16</sup> (see Fig. 4c). In fact, clearly distinguishable clustering of polysulfide (blue) and Li-F (red) species supports this multiphase structural view of the SEI layer. However, significant overlapping of polysulfide and Li-F regions (black) reveals the presence of a matrix type SEI layer with continuous phases and diffuse boundaries between the various sulfide and fluoride based regimes (see Fig. 4d). The simultaneous multiphase and continuous phase SEI layer formation can be explained by the Stranski–Krastanov (SK) growth model developed for thin film nucleation processes.<sup>67</sup> Based on this growth model, the SEI layer formation can be viewed as a two-step process where a) the products of parasitic reactions at the Li-anode surface result in multiphase layers (such as  $\text{Li}_2\text{S}$ ,  $\text{Li}_2\text{O}$  and LiF), and b) clustering of transient species from parasitic reactions, by strongly interacting with the electrolyte and other SEI components, leads to a matrix type precipitation. During the evolution of first step, the parasitic products need to be adjacent to the Li-anode surface to gain expedited access to preferably unbound  $\text{Li}^+$  ions that can facilitate an extended network of  $\text{Li}_2\text{S}$  and LiF solid multiphase layers. For example, clustering of polysulfide as part of the shuttling process on the Li-anode can cause the nucleation of  $\text{Li}_2\text{S}$  phases by accessing the Li stripping process during discharge cycles. With growth to critical thickness, this insoluble multiphase layer can significantly inhibit the access to unbound  $\text{Li}^+$  from the Li-anode and thereby activate the second stage of the SEI layer growth. With restricted access to the Li-metal surface and scarcity of unbound  $\text{Li}^+$  ions, the parasitic reaction products will react with each other as well as with adjacent electrolyte components to initiate nucleation directly on the multiphase layer and produce a matrix type phase with diffused boundaries. In particular, the restricted access to Li-metal can cause partial polysulfide reduction processes (Eq.3) leading to a mono-anionic polysulfide ( $\text{LiS}_5$ ) as a major component of the secondary layer that results in a

1  
2  
3 high  $S_B^0/S_T^{1-}$  ratio ( $\geq 3$ ). This secondary SEI layer  
4 mainly consists of aggregated polysulfides and  
5 oligomeric reactive products, and is comparable to  
6 the organic phase layer comprised of polymerized  
7 solvents reported in lithium-ion batteries.<sup>13, 59, 66</sup>  
8 Nevertheless, the major difference is that it involves  
9 polysulfides as a main component and also serves as  
10 absorbent layer for the shuttling polysulfides, which  
11 leads to an exponential increase in polysulfides after  
12 the first charge/discharge cycle in high resolution in-  
13 situ XPS (see Fig. 2b). In addition, the adsorbed  
14 polysulfides can undergo association and  
15 disproportionation reactions causing oligomeric  
16 aggregates on top of the SEI layer, which is evident  
17 from the clustering of polysulfides detected via in-  
18 situ imaging XPS analysis (see Fig. 4b).<sup>38</sup> Unlike the  
19 primary multiphase layer containing inorganic solid  
20 phases, the constituents of the second stage matrix-  
21 type layer could be relatively soluble and hence  
22 subsequent polysulfide fouling will be a dynamic  
23 process depending on electrolyte composition and  
24 cycling current rate. In short, the oligomeric  
25 aggregation of polysulfides on the SEI layer entraps  
26 the active material on the Li-anode and manifests as  
27 the severe capacity fading that is widely reported in  
28 the Li-S battery literature. To this end, our study  
29 suggests that effective Li-metal protection requires  
30 careful design of protective scaffolds, which not only  
31 prevent the inorganic multiphase primary layer but  
32 also inhibit the polysulfide fouling process.

### 33 Conclusions

34  
35 In summary, in-situ XPS and computational  
36 modeling studies were carried out on a model Li-S  
37 battery system to understand the growth mechanism  
38 of the SEI layer on the Li-anode. The XPS core level  
39 spectra of S 2p showed a gradual increase of sulfide  
40 dianion ( $S^{2-}$ ) indicating the formation of insoluble  
41 and electronically insulating  $Li_2S$  due to polysulfide  
42 reduction processes. Similarly, the F 1s spectra  
43 showed a significant increase in Li-F and C-F species  
44 with a decrease in  $CF_3$  (associated with pristine TFSI  
45 anion) indicating its decomposition in the proximity  
46 of the Li-anode. Evolution of both  $Li_2S$  and Li-F  
47 species with cycling causes the precipitation of an  
48 inorganic multiphase layer as the primary SEI  
49 component. A simultaneous exponential increase of  
50 polysulfide species ( $S^0$  and  $S^{1-}$ ) suggests a continuous  
51 fouling process on the Li anode during both charge  
52 and discharge cycles. The high  $S_B^0/S_T^{1-}$  ratio ( $>3$ )  
53 observed for the polysulfide species involved in this  
54 fouling process indicates the formation of mono-  
55 anionic polysulfide (i.e.  $LiS_5$ ) due to restricted access  
56 to Li-metal during the sulfide reduction process.  
57 With access to the Li-metal surface becoming  
58 restricted, the parasitic reaction products (fluoride  
59  
60

and sulfide anions) will engage in cross-interaction  
with adjacent electrolyte components and nucleate  
into a secondary matrix type SEI layer, which is  
visualized as clustering in XPS imaging and  
supported by AIMD analysis. The continuous  
increase in polysulfide concentration at the Li-anode  
interface also suggests a facilitated fouling process  
due to its absorption on a matrix type SEI layer.  
Chemical entrapment of the dissolved polysulfides at  
the top of the matrix type layer on the Li-anode  
causes the fouling and subsequent continuous loss of  
active material, leading to the severe capacity fading  
widely observed in Li-S battery technologies.  
Ultimately, controlling the role of SEI layer in Li-S  
batteries will require a multi-functional scaffold  
design, which can deflect the shuttling polysulfide as  
well as inhibit the electrolyte decomposition on Li-  
anode surfaces.

### Acknowledgements

The in-situ XPS cell designs were funded by the  
Chemical Imaging Initiative as part of the Laboratory  
Directed Research and Development (LDRD)  
program at Pacific Northwest National Laboratory  
(PNNL). The Li-S battery materials and  
measurements were funded through the Joint Center  
for Energy Storage Research (JCESR) sponsored by  
Department of Energy Basic Energy Science (DOE-  
BES) program. The in-situ XPS characterization was  
carried out in the Environmental Molecular Sciences  
Laboratory (EMSL), a DOE Office of Science User  
Facility sponsored by the Office of Biological and  
Environmental Research and located at PNNL. LECF  
and PBB acknowledge financial support from the  
Assistant Secretary for Energy Efficiency and  
Renewable Energy, Office of Vehicle Technologies  
of the U.S. Department of Energy under Contract No.  
DE-EE0006832 under the Advanced Battery  
Materials Research (BMR) Program. Supercomputer  
resources from Texas A&M University High  
Performance Computer Center and Texas Advanced  
Computing Center (TACC) are gratefully  
acknowledged. VM and PB thank Dr. Nav Nidhi  
Rajput, LBNL for fruitful discussions regarding  
computational modeling results.

### ASSOCIATED CONTENT

Supporting Information. Supporting information  
includes detailed experimental procedures on  
synthesis of  $Li_2S_6$  electrolyte, in-situ XPS cell  
design and analysis, and DFT and AIMD simulation  
studies. This material is available for free of charge  
via the Internet at <http://pubs.acs.org>.

## AUTHOR INFORMATION

### Corresponding Author

\* (VM) Email: [vijay@pnnl.gov](mailto:vijay@pnnl.gov); Tel: (509)-371-6540

ORCID: Vijayakumar Murugesan [0000-0001-6149-1702](https://orcid.org/0000-0001-6149-1702)

### Present Addresses

†Department of Physics, Montana State University, Bozeman, MT 59717.

## References

- Barghamadi, M.; Kapoor, A.; Wen, C., A Review on Li-S Batteries as a High Efficiency Rechargeable Lithium Battery. *J. Electrochem. Soc.* 2013, 160, A1256-A1263.
- Bruce, P. G.; Freunberger, S. A.; Hardwick, L. J.; Tarascon, J.-M., Li-O<sub>2</sub> and Li-S batteries with high energy storage. *Nat. Mater.* 2012, 11, 19-29.
- Ji, X.; Nazar, L. F., Advances in Li-S batteries. *J. Mater. Chem.* 2010, 20, 9821-9826.
- Lin, Z.; Liang, C., Lithium-sulfur batteries: from liquid to solid cells. *J. Mater. Chem. A* 2015, 3, 936-958.
- Yin, Y.-X.; Xin, S.; Guo, Y.-G.; Wan, L.-J., Lithium-Sulfur Batteries: Electrochemistry, Materials, and Prospects. *Angew. Chem., Int. Ed.* 2013, 52, 13186-13200.
- Budi, A.; Basile, A.; Opletal, G.; Hollenkamp, A. F.; Best, A. S.; Rees, R. J.; Bhatt, A. I.; O'Mullane, A. P.; Russo, S. P., Study of the Initial Stage of Solid Electrolyte Interphase Formation upon Chemical Reaction of Lithium Metal and N-Methyl-N-Propyl-Pyrrolidinium-Bis(Fluorosulfonyl)Imide. *J. Phys. Chem. C* 2012, 116, 19789-19797.
- Markevich, E.; Salitra, G.; Rosenman, A.; Talyosef, Y.; Chesneau, F.; Aurbach, D., The effect of a solid electrolyte interphase on the mechanism of operation of lithium-sulfur batteries. *J. Mater. Chem. A* 2015, 3, 19873-19883.
- Cheon, S.-E.; Choi, S.-S.; Han, J.-S.; Choi, Y.-S.; Jung, B.-H.; Lim, H. S., Capacity Fading Mechanisms on Cycling a High-Capacity Secondary Sulfur Cathode. *J. Electrochem. Soc.* 2004, 151, A2067-A2073.
- Diao, Y.; Xie, K.; Xiong, S.; Hong, X., Insights into Li-S Battery Cathode Capacity Fading Mechanisms: Irreversible Oxidation of Active Mass during Cycling. *J. Electrochem. Soc.* 2012, 159, A1816-A1821.
- Barchasz, C.; Molton, F.; Duboc, C.; Leprière, J.-C.; Patoux, S.; Alloin, F., Lithium/Sulfur Cell Discharge Mechanism: An Original Approach for Intermediate Species Identification. *Anal. Chem.* 2012, 84, 3973-3980.
- Liu, Z.; Bertolini, S.; Balbuena, P. B.; Mukherjee, P. P., Li<sub>2</sub>S Film Formation on Lithium Anode Surface of Li-S batteries. *ACS Appl. Mater. Interfaces* 2016, 8, 4700-4708.
- Li, Y.; Leung, K.; Qi, Y., Computational Exploration of the Li-Electrode|Electrolyte Interface in the Presence of a Nanometer Thick Solid-Electrolyte Interphase Layer. *Acc. Chem. Res.* 2016, 49, 2363-2370.
- An, S. J.; Li, J.; Daniel, C.; Mohanty, D.; Nagpure, S.; Wood Iii, D. L., The state of understanding of the lithium-ion-battery graphite solid electrolyte interphase (SEI) and its relationship to formation cycling. *Carbon* 2016, 105, 52-76.
- Gauthier, M.; Carney, T. J.; Grimaud, A.; Giordano, L.; Pour, N.; Chang, H.-H.; Fenning, D. P.; Lux, S. F.; Paschos, O.; Bauer, C.; Maglia, F.; Lupart, S.; Lamp, P.; Shao-Horn, Y., Electrode-Electrolyte Interface in Li-Ion Batteries: Current Understanding and New Insights. *J. Phys. Chem. Lett.* 2015, 6, 4653-4672.
- Ganesh, P.; Kent, P. R. C.; Jiang, D.-e., Solid-Electrolyte Interphase Formation and Electrolyte Reduction at Li-Ion Battery Graphite Anodes: Insights from First-Principles Molecular Dynamics. *J. Phys. Chem. C* 2012, 116, 24476-24481.
- Leung, K.; Soto, F.; Hankins, K.; Balbuena, P. B.; Harrison, K. L., Stability of Solid Electrolyte Interphase Components on Lithium Metal and Reactive Anode Material Surfaces. *J. Phys. Chem. C* 2016, 120, 6302-6313.

## Author Contributions

The manuscript was written through contributions of all authors. M. I. N., A. M. S., S.T., and V. S. conducted the in-situ XPS analysis, L. E. C. and P. B. B. carried out the DFT and AIMD simulation studies. V.M, and K. T. M. designed and supervised the project.

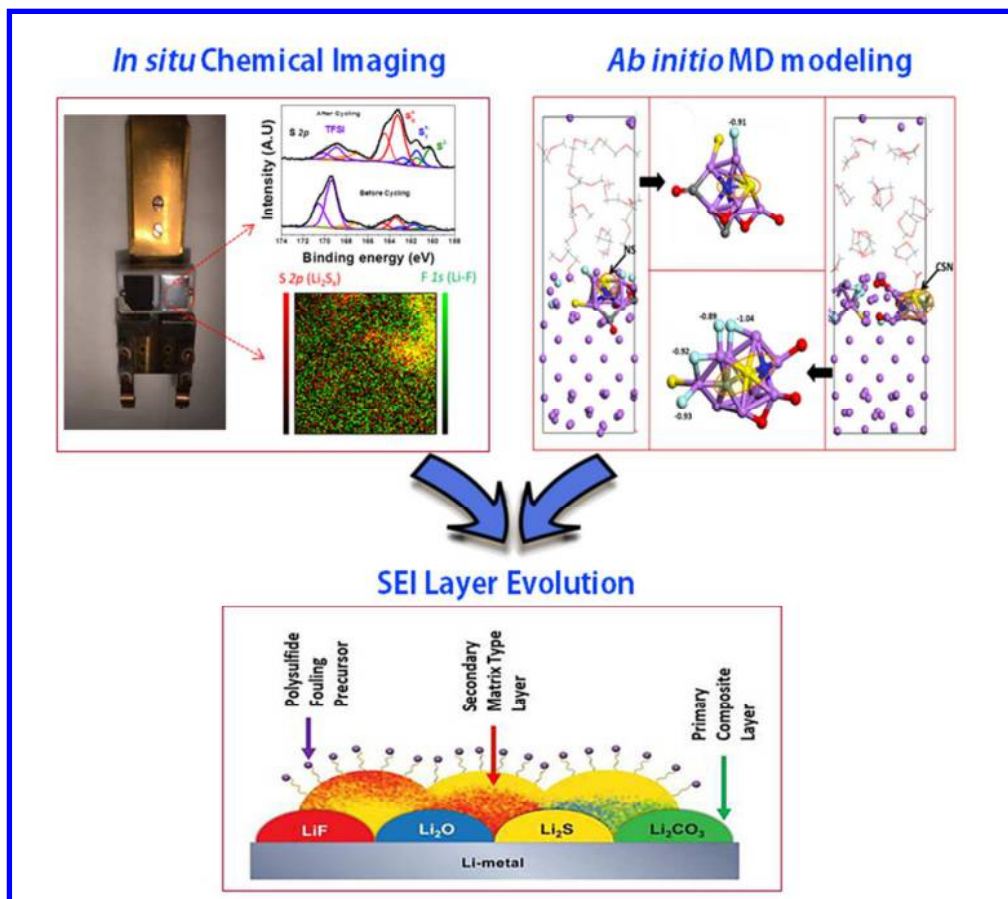
## Notes

The authors declare no competing financial interest.

17. Ebadi, M.; Brandell, D.; Araujo, C. M., Electrolyte decomposition on Li-metal surfaces from first-principles theory. *J. Chem. Phys.* 2016, 145, 204701.
18. Chen, X.; Hou, T.-Z.; Li, B.; Yan, C.; Zhu, L.; Guan, C.; Cheng, X.-B.; Peng, H.-J.; Huang, J.-Q.; Zhang, Q., Towards stable lithium-sulfur batteries: Mechanistic insights into electrolyte decomposition on lithium metal anode. *Energy Storage Materials*, 2017, In press
19. Harks, P. P. R. M. L.; Mulder, F. M.; Notten, P. H. L., In situ methods for Li-ion battery research: A review of recent developments. *J. Power Sources* 2015, 288, 92-105.
20. Hagen, M.; Schiffels, P.; Hammer, M.; Dörfler, S.; Tübke, J.; Hoffmann, M. J.; Althues, H.; Kaskel, S., In-Situ Raman Investigation of Polysulfide Formation in Li-S Cells. *J. Electrochem. Soc.* 2013, 160, A1205-A1214.
21. Patel, M. U. M.; Demir-Cakan, R.; Morcrette, M.; Tarascon J.-M.; Gaberscek, M.; Dominko, R., Li-S Battery Analyzed by UV/Vis in Operando Mode. *ChemSusChem* 2013, 6, 1177-1181.
22. Wang, Q.; Zheng, J.; Walter, E.; Pan, H.; Lv, D.; Zuo, P.; Chen, H.; Deng, Z. D.; Liaw, B. Y.; Yu, X.; Yang, X.; Zhang, J.-G.; Liu, J.; Xiao, J., Direct Observation of Sulfur Radicals as Reaction Media in Lithium Sulfur Batteries. *J. Electrochem. Soc.* 2015, 162, A474-A478.
23. Cuisinier, M.; Cabelguen, P.-E.; Evers, S.; He, G.; Kolbeck, M.; Garsuch, A.; Bolin, T.; Balasubramanian, M.; Nazar, L. F., Sulfur Speciation in Li-S Batteries Determined by Operando X-ray Absorption Spectroscopy. *J. Phys. Chem. Lett.* 2013, 4, 3227-3232.
24. Lowe, M. A.; Gao, J.; Abruna, H. D., Mechanistic insights into operational lithium-sulfur batteries by in situ X-ray diffraction and absorption spectroscopy. *RSC Advan.* 2014, 4, 18347-18353.
25. Patel, M. U. M.; Arčon, I.; Aquilanti, G.; Stievano, L.; Mali, G.; Dominko, R., X-ray Absorption Near-Edge Structure and Nuclear Magnetic Resonance Study of the Lithium-Sulfur Battery and its Components. *ChemPhysChem* 2014, 15, 894-904.
26. Wujcik, K. H.; Pascal, T. A.; Pemmaraju, C. D.; Devaux, D.; Stolte, W. C.; Balsara, N. P.; Prendergast, D., Characterization of Polysulfide Radicals Present in an Ether-Based Electrolyte of a Lithium-Sulfur Battery During Initial Discharge Using In Situ X-Ray Absorption Spectroscopy Experiments and First-Principles Calculations. *Adv. Energy Mater.* 2015, 5, 1500285.
27. See, K. A.; Leskes, M.; Griffin, J. M.; Britto, S.; Matthews, P. D.; Emly, A.; Van der Ven, A.; Wright, D. S.; Morris, A. J.; Grey, C. P.; Seshadri, R., Ab Initio Structure Search and in Situ 7Li NMR Studies of Discharge Products in the Li-S Battery System. *J. Am. Chem. Soc.* 2014, 136, 16368-16377.
28. Xiao, J.; Hu, J. Z.; Chen, H.; Vijayakumar, M.; Zheng, J.; Pan, H.; Walter, E. D.; Hu, M.; Deng, X.; Feng, J.; Liaw, B. Y.; Gu, M.; Deng, Z. D.; Lu, D.; Xu, S.; Wang, C.; Liu, J., Following the Transient Reactions in Lithium-Sulfur Batteries Using an In Situ Nuclear Magnetic Resonance Technique. *Nano Lett.* 2015, 15, 3309-3316.
29. Lin, C.-N.; Chen, W.-C.; Song, Y.-F.; Wang, C.-C.; Tsai, L.-D.; Wu, N.-L., Understanding dynamics of polysulfide dissolution and re-deposition in working lithium-sulfur battery by in-operando transmission X-ray microscopy. *J. Power Sources* 2014, 263, 98-103.
30. Nelson, J.; Misra, S.; Yang, Y.; Jackson, A.; Liu, Y.; Wang, H.; Dai, H.; Andrews, J. C.; Cui, Y.; Toney, M. F., In Operando X-ray Diffraction and Transmission X-ray Microscopy of Lithium Sulfur Batteries. *J. Am. Chem. Soc.* 2012, 134, 6337-6343.
31. Yu, X.; Pan, H.; Zhou, Y.; Northrup, P.; Xiao, J.; Bak, S.; Liu, M.; Nam, K.-W.; Qu, D.; Liu, J.; Wu, T.; Yang, X.-Q., Direct Observation of the Redistribution of Sulfur and Polysulfides in Li-S Batteries During the First Cycle by In Situ X-Ray Fluorescence Microscopy. *Adv. Energy Mater.* 2015, 5, 1500072.
32. Lin, D.; Liu, Y.; Cui, Y., Reviving the lithium metal anode for high-energy batteries. *Nat. Nano* 2017, 12, 194-206.
33. Barghamadi, M.; Best, A. S.; Bhatt, A. I.; Hollenkamp, A. F.; Mahon, P. J.; Musameh, M.; Rütther, T., Effect of Anion on Behaviour of Li-S Battery Electrolyte Solutions Based on N-Methyl-N-Butyl-Pyrrolidinium Ionic Liquids. *Electrochim. Acta* 2015, 180, 636-644.
34. Vranes, M.; Dozic, S.; Djeric, V.; Gadzuric, S., Physicochemical Characterization of 1-Butyl-3-methylimidazolium and 1-Butyl-1-methylpyrrolidinium Bis(trifluoromethylsulfonyl)imide. *J. Chem. Eng. Data* 2012, 57, 1072-1077.
35. Zheng, J.; Gu, M.; Chen, H.; Meduri, P.; Engelhard, M. H.; Zhang, J.-G.; Liu, J.; Xiao, J., Ionic liquid-enhanced solid state electrolyte interface (SEI) for lithium-sulfur batteries. *Journal of Materials Chemistry A* 2013, 1, 8464-8470.
36. Höfft, O.; Krischok, S., Vacuum Electrochemistry in Ionic Liquids. *Electrochemical Society Interface* 2014, 53.
37. Paulechka, Y. U.; Zaitsau, D. H.; Kabo, G. J.; Strechan, A. A., Vapor pressure and thermal

- 1  
2  
3 stability of ionic liquid 1-butyl-3-  
4 methylimidazolium  
5 Bis(trifluoromethylsulfonyl)amide. *Thermochimi.*  
6 *Acta* 2005, 439, 158-160.
- 7 38. Vijayakumar, M.; Govind, N.; Walter, E.; Burton,  
8 S. D.; Shukla, A.; Devaraj, A.; Xiao, J.; Liu, J.;  
9 Wang, C.; Karim, A.; Thevuthasan, S., Molecular  
10 structure and stability of dissolved lithium  
11 polysulfide species. *Phy. Chem. Chem. Phys.* 2014,  
12 16, 10923-10932.
- 13 39. Frisch, M. J.; Trucks, G. W.; Schlegel, H. B.;  
14 Scuseria, G. E.; Robb, M. A.; Cheeseman, J. R.;  
15 Scalmani, G.; Barone, V.; Mennucci, B.;  
16 Petersson, G. A.; Nakatsuji, H.; Caricato, M.; Li,  
17 X.; Hratchian, H. P.; Izmaylov, A. F.; Bloino, J.;  
18 Zheng, G.; Sonnenberg, J. L.; Hada, M.; Ehara,  
19 M.; Toyota, K.; Fukuda, R.; Hasegawa, J.; Ishida,  
20 M.; Nakajima, T.; Honda, Y.; Kitao, O.; Nakai,  
21 H.; Vreven, T.; Montgomery Jr., J. A.; Peralta, J.  
22 E.; Ogliaro, F. o.; Bearpark, M. J.; Heyd, J.;  
23 Brothers, E. N.; Kudin, K. N.; Staroverov, V. N.;  
24 Kobayashi, R.; Normand, J.; Raghavachari, K.;  
25 Rendell, A. P.; Burant, J. C.; Iyengar, S. S.;  
26 Tomasi, J.; Cossi, M.; Rega, N.; Millam, N. J.;  
27 Klene, M.; Knox, J. E.; Cross, J. B.; Bakken, V.;  
28 Adamo, C.; Jaramillo, J.; Gomperts, R.;  
29 Stratmann, R. E.; Yazyev, O.; Austin, A. J.;  
30 Cammi, R.; Pomelli, C.; Ochterski, J. W.; Martin,  
31 R. L.; Morokuma, K.; Zakrzewski, V. G.; Voth,  
32 G. A.; Salvador, P.; Dannenberg, J. J.; Dapprich,  
33 S.; Daniels, A. D.; Farkas, A. d. n.; Foresman, J.  
34 B.; Ortiz, J. V.; Cioslowski, J.; Fox, D. J.  
35 Gaussian 09, Gaussian, Inc.: Wallingford, CT,  
36 USA, 2009.
- 37 40. Tomasi, J.; Mennucci, B.; Cammi, R., Quantum  
38 Mechanical Continuum Solvation Models. *Chem.*  
39 *Rev.* 2005, 105, 2999-3094.
- 40 41. Camacho-Forero, L. E.; Smith, T. W.; Bertolini,  
41 S.; Balbuena, P. B., Reactivity at the Lithium–  
42 Metal Anode Surface of Lithium–Sulfur Batteries.  
43 *J. Phy. Chem. C* 2015, 119, 26828-26839.
- 44 42. Kresse, G.; Furthmuller, J., Efficiency of ab-initio  
45 total energy calculations for metals and  
46 semiconductors using a plane-wave basis set.  
47 *Computational Materials Science* 1996, 6 (1), 15-  
48 50.
- 49 43. Kresse, G.; Hafner, J., Ab initio molecular  
50 dynamics for liquid metals. *Phy. Rev. B* 1993, 47,  
51 558-561.
- 52 44. Perdew, J. P.; Burke, K.; Ernzerhof, M.,  
53 Generalized Gradient Approximation Made  
54 Simple. *Phy. Rev. Lett.* 1996, 77, 3865-3868.
- 55 45. Blöchl, P. E., Projector augmented-wave method.  
56 *Phy. Rev. B* 1994, 50, 17953-17979.
- 57 46. Kresse, G.; Joubert, D., From ultrasoft  
58 pseudopotentials to the projector augmented-wave  
59 method. *Phy. Rev. B* 1999, 59, 1758-1775.
- 60 47. Tang, W.; Sanville, E.; Henkelman, G., A grid-  
based Bader analysis algorithm without lattice  
bias. *J. Phy. Cond. Mat.* 2009, 21, 084204.
48. Sanville, E.; Kenny, S. D.; Smith, R.; Henkelman,  
G., Improved grid-based algorithm for Bader  
charge allocation. *J. Comput. Chem.* 2007, 28,  
899-908.
49. Henkelman, G.; Arnaldsson, A.; Jónsson, H., A  
fast and robust algorithm for Bader decomposition  
of charge density. *Comput. Mater. Sci.* 2006, 36  
(3), 354-360.
50. Men, S.; Lovelock, K. R. J.; Licence, P., X-ray  
photoelectron spectroscopy of pyrrolidinium-  
based ionic liquids: cation-anion interactions and  
a comparison to imidazolium-based analogues.  
*Phys. Chem. Chem. Phys.* 2011, 13 (33), 15244-  
15255.
51. Smart, R. S. C.; Skinner, W. M.; Gerson, A. R.,  
XPS of sulphide mineral surfaces: metal-deficient,  
polysulphides, defects and elemental sulphur.  
*Surf. Interface Anal.* 1999, 28 (1), 101-105.
52. Liang, X.; Hart, C.; Pang, Q.; Garsuch, A.; Weiss,  
T.; Nazar, L. F., A highly efficient polysulfide  
mediator for lithium–sulfur batteries. *Nat.*  
*Commun.* 2015, 6.
53. Turner, N. H.; Murday, J. S.; Ramaker, D. E.,  
Quantitative determination of surface composition  
of sulfur bearing anion mixtures by Auger  
electron spectroscopy. *Anal. Chem.* 1980, 52, 84-  
92.
54. Fantauzzi, M.; Elsener, B.; Atzei, D.; Rigoldi, A.;  
Rossi, A., Exploiting XPS for the identification of  
sulfides and polysulfides. *RSC Advances* 2015, 5,  
75953-75963.
55. Assary, R. S.; Curtiss, L. A.; Moore, J. S., Toward  
a Molecular Understanding of Energetics in Li–S  
Batteries Using Nonaqueous Electrolytes: A High-  
Level Quantum Chemical Study. *J. Phys. Chem. C*  
2014, 118, 11545-11558.
56. Li, W.; Yao, H.; Yan, K.; Zheng, G.; Liang, Z.;  
Chiang, Y.-M.; Cui, Y., The synergetic effect of  
lithium polysulfide and lithium nitrate to prevent  
lithium dendrite growth. *Nat. Commun.* 2015, 6,  
7436.
57. Bhattacharya, P.; Nandasiri, M. I.; Lv, D.;  
Schwarz, A. M.; Darsell, J. T.; Henderson, W. A.;  
Tomalia, D. A.; Liu, J.; Zhang, J.-G.; Xiao, J.,  
Polyamidoamine dendrimer-based binders for  
high-loading lithium–sulfur battery cathodes.  
*Nano Energy* 2016, 19, 176-186.
58. Howlett, P. C.; Brack, N.; Hollenkamp, A. F.;  
Forsyth, M.; MacFarlane, D. R., Characterization  
of the Lithium Surface in N-Methyl-N-

- 1  
2  
3 alkylypyrrolidinium  
4 Bis(trifluoromethanesulfonyl)amide Room-  
5 Temperature Ionic Liquid Electrolytes. *J.*  
6 *Electrochem. Soc.* 2006, 153, A595-A606.
- 7 59. Cheng, X.-B.; Zhang, R.; Zhao, C.-Z.; Wei, F.;  
8 Zhang, J.-G.; Zhang, Q., A Review of Solid  
9 Electrolyte Interphases on Lithium Metal Anode.  
10 *Advan. Sci.* 2016, 3 (3), 1500213-n/a.
- 11 60. Xu, C.; Sun, B.; Gustafsson, T.; Edstrom, K.;  
12 Brandell, D.; Hahlin, M., Interface layer formation  
13 in solid polymer electrolyte lithium batteries: an  
14 XPS study. *J. Mater. Chem. A* 2014, 2 (20), 7256-  
15 7264.
- 16 61. Chan, C. K.; Ruffo, R.; Hong, S. S.; Cui, Y.,  
17 Surface chemistry and morphology of the solid  
18 electrolyte interphase on silicon nanowire lithium-  
19 ion battery anodes. *J. Power Sources* 2009, 189  
20 (2), 1132-1140.
- 21 62. Schroder, K. W.; Celio, H.; Webb, L. J.;  
22 Stevenson, K. J., Examining Solid Electrolyte  
23 Interphase Formation on Crystalline Silicon  
24 Electrodes: Influence of Electrochemical  
25 Preparation and Ambient Exposure Conditions. *J.*  
26 *Phys. Chem. C* 2012, 116, 19737-19747.
- 27 63. Leroy, S.; Martinez, H.; Dedryvère, R.;  
28 Lemordant, D.; Gonbeau, D., Influence of the  
29 lithium salt nature over the surface film formation  
30 on a graphite electrode in Li-ion batteries: An  
31 XPS study. *Appl. Surf. Sci.* 2007, 253, 4895-4905.
- 32 64. Song, J.; Noh, H.; Lee, H.; Lee, J.-N.; Lee, D. J.;  
33 Lee, Y.; Kim, C. H.; Lee, Y. M.; Park, J.-K.; Kim,  
34 H.-T., Polysulfide rejection layer from alpha-  
35 lipoic acid for high performance lithium-sulfur  
36 battery. *J. Mater. Chem. A* 2015, 3, 323-330.
- 37 65. Nguyen, C. C.; Woo, S.-W.; Song, S.-W.,  
38 Understanding the Interfacial Processes at  
39 Silicon-Copper Electrodes in Ionic Liquid Battery  
40 Electrolyte. *J. Phys. Chem. C* 2012, 116 (28),  
41 14764-14771.
- 42 66. Soto, F. A.; Ma, Y.; Martinez de la Hoz, J. M.;  
43 Seminario, J. M.; Balbuena, P. B., Formation and  
44 Growth Mechanisms of Solid-Electrolyte  
45 Interphase Layers in Rechargeable Batteries.  
46 *Chem. Mater.* 2015, 27, 7990-8000.
- 47 67. Venables, J. A.; Spiller, G. D. T.; Hanbucken, M.,  
48 Nucleation and growth of thin films. *Rep. Prog.*  
49 *Phys.* 1984, 47, 399.
- 50 68. Gurker, N.; Ebel, M. F.; Ebel, H.; Mantler, M.;  
51 Hedrich, H.; Schön, P., Imaging XPS—a new  
52 technique. 2—Experimental verification. *Surf.*  
53 *Interface Anal.* 1987, 10, 242-249.
- 54 69. Gurker, N.; Ebel, M. F.; Ebel, H., Imaging XPS—  
55 A new technique, I—principles. *Surf. Interface*  
56 *Anal.* 1983, 5, 13-19.
- 57  
58  
59  
60



Molecules to Mesoscale – A Multimodal View of SEI layer Evolution in Li-S Battery

215x190mm (96 x 96 DPI)